Closed Loop Control of a Pulsed Series Parallel Resonant Converter with Current Doubler

K. Klement, H. Timborabadi, A. El-Deib and F. Dawson

Department of Electrical and Computer Engineering, University of Toronto, Toronto ON, M5S 3G4, Canada

Abstract-- **In this paper a series-parallel resonant converter with a current doubler at the output is designed to produce a pulsed voltage to feed an electrochemical waste water treatment cell. The small signal model of the converter is derived to design the compensators of a cascaded control loop with an inner current and an outer voltage loop. The design procedure of the compensators in the control loop is also demonstrated. To avoid any measurements at the electrochemical cell the output voltage and current are estimated through the measured signals on the high voltage, low current primary side. Simulation and experimental results are given to validate the operation of the power supply under pulsed operation.**

Index Terms-- **resonant converter, controller design, pulsed power**

I. INTRODUCTION

Electrochemical wastewater treatment is conventionally performed as a steady state process, whereby the system is operated at one voltage or current set point. However, it is possible to make gains in the efficiency of the process by pulsing the waveform rather than operating in steady state. The largest body of literature available on pulsed electrochemical processes is on pulsed plating, which is a pulsed form of electrodeposition commonly used for electric contacts and printed circuit boards.

In electrodeposition, a conductive object is placed in an electrolyte bath containing metal ions and a current is passed between that object and an anode. The current reduces metal ions in the solution so that the metal deposits onto the object. Generally, this process uses a direct current, but pulse electrodeposition (PED) is also used. In PED, the current is pulsed in either a unipolar sense (on then off) or a bipolar sense (positive then negative).

The advantages of PED are as follows:
1. The double layer at the cathode surface discharges between pulses so that there is less obstruction to ion flow from the solution to the electrode [1] and adsorption and desorption can occur more easily [2].
2. It there is uneven current distribution and therefore uneven ion depletion in the electrolyte, ions are able to migrate to the depleted portions during the off time so that they are distributed more evenly over the electrode surface [1]. This is a significant advantage for plating because it increases "throwing power", the ability of a solution to deposit into recessed areas.

To obtain the same average current density as in the dc case, much higher instantaneous current densities are achieved. Higher instantaneous current density causes higher overpotential at the electrode, which influences which reactions occur and the ratio in which reactions of different kinetics occur [2]. Therefore, it is possible to improve the current efficiency of a desirable reaction (the percentage of total current that goes into that reaction) by pulsing.

According to Chandrasekar [1], the primary disadvantages of PED are (i) increased cost of the power supply and (ii) more planning required for developing a process control algorithm since there are three variables to set (current amplitude, on time, and off time) rather than one (current amplitude).

In selecting the three variables for pulse electrolysis, two primary effects must be taken into consideration: (i) charging of the double layer and (ii) mass transport effects. Detailed analysis of these phenomena can be found in references [2]-[6].

Chandrasekar's reference to increased power supply cost is based on the conventional approaches of providing high current at low voltage. The conventional power supplies are bulky and the bus work between individual plate systems is awkward. Pulsing introduces an additional element of complexity which existing designs have difficulty in addressing since the dynamic response of the existing systems is slow. This paper proposes an alternative power supply design approach which is less costly and has a number of additional advantages which will be described.

The anode and cathode plates in many electrochemical/electrodeposition processes are typically connected in series and in parallel. The optimum series parallel configuration is based on a number of factors related to the process which is beyond the scope of this paper. Suffice to say that the output requirements are typically high current at low voltage. The optimized cell structures or stacks are then connected to individual power sources. Each of these power sources should in principle be galvanically isolated.

In designing a power source for a stack it is necessary to take into account the following requirements: minimizing the amount of stored energy in the event of a fault in the cell, maintaining a low output ripple current, the ability to parallel and achieve higher powers (modularity and increased availability), fast dynamic response under pulsed conditions, high efficiency operation and inexpensive and robust sensing circuitry

for protection and control. The first five requirements imply the use of small energy storage components and a switch mode power supply that operates at high frequencies. Higher efficiency is achieved by exploiting resonance structures that minimize switching losses. These resonant power supplies operate from a dc voltage supply and have an upper bound on their power rating. In general, many supplies need to be placed in parallel to meet the output current requirements. Hence, the dc-dc power supplies are distributed but operate from a common dc bus.

In this paper we explore the use of a resonant current doubler to provide pulsed power to an electrochemical load. The current doubler approach is attractive for the following reasons: synchronous rectification can be implemented quite simply to achieve higher efficiency, a simple planar transformer design can be implemented, the output dc filter consists of only two dc chokes each rated at half the rated output dc current in contrast to a series resonant structure which would require a dc output filter with high rms current output capacitors as well as a dc choke. An LC filter combination is required in a series resonant structure in order to reduce the amount of ripple current flowing through the electrochemical cell.

The model of the electrochemical load has been simplified since the details of this type of load, specifically the dynamics, are still not well understood. Nevertheless, the model which is used in this paper can replicate the salient features of an electrochemical load.

The main contributions of this paper are (a) a closed loop control model for the current doubler assuming pulsed dc operating conditions and (b) the implementation of an output dc current and voltage estimation scheme that relies on a sensed current and voltage on the high voltage low current ac side of the resonant converter converter. The implementation of a high current dc sensor is more costly. Moreover, signal isolation and isolated power supplies would be required to operate sensors which are situated on the dc side.

II. SERIES PARALLEL RESONANT CONVERTER WITH CURRENT DOUBLER

The model used to represent the electrochemical load is shown in Fig. 1. R_{int} (15 mΩ) and C_{dl} (250 F) represent the faradaic resistance and space charge capacitance of the electrode/electrolyte interfacial zone respectively. R_{elec} represents the electrolyte resistance which is 20 mΩ. The rated output dc voltage and output dc current are 5 V and 100 A respectively.

The series parallel resonant converter (SPRC) with current doubler circuit which has been simulated and experimentally verified is shown in Fig. 2. The load in Fig. 2 is shown as R_{eq} (50 mΩ) however the circuit was also tested with the simplified representation of the aforementioned electrochemical load shown in Fig. 1.
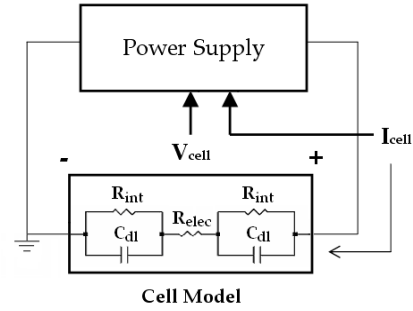

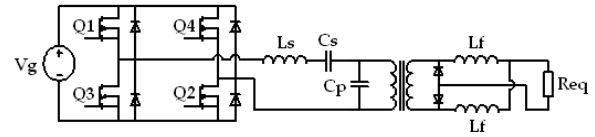Fig. 1 Power supply connected to a rudimentary model of an electrochemical load.

Fig. 2 Series parallel resonant converter with current doubler

A. Nonlinear State Space Model

The circuit under study is shown in Figure 2. As for the SRC case, the nonlinear load will be represented by an equivalent resistance and the magnetizing current will be neglected since it is much smaller than the resonant tank current (2 orders of magnitude).

The small signal model has been derived using the generalized averaging approach described in [8]. The nonlinear differential equations for this system are as follows:

$$\frac{d}{dt}i_{Ls} = \frac{1}{L_s}\left\{-v_{Cs} - v_{Cp} + V_s \, \text{sgn}(\sin(\omega_s t))\right\} \tag{1}$$

$$\frac{d}{dt}v_{Cs} = \frac{1}{C_s}i_{Ls} \tag{2}$$

$$\frac{d}{dt}v_{Cp} = \frac{1}{C_p}\left\{i_{Ls} - i_o \, \text{sgn}(v_{Cp})\right\} \tag{3}$$

$$\frac{d}{dt}i_{Lf} = \frac{1}{L_f}\left\{\frac{1}{2}abs(v_{Cp}) - 2i_{Lf}R\right\} \tag{4}$$

In the above equations, i_{Ls} is the series inductance current, v_{Cs} is the series capacitor voltage, v_{Cp} is the parallel capacitor voltage and i_{Lf} is the filter inductance current. The steady state operation and open loop control response of the current doubler has been reported in the literature [7]. The small signal model used in the controller design procedure is obtained by linearizing the system (1)-(4) around the operating point to obtain the control-to-output transfer functions:

$$\frac{\hat{i}_o(s)}{\hat{\omega}_s(s)} = \begin{bmatrix} 0 & 0 & 0 & 0 & 0 & 0 & 2 \end{bmatrix}(sI-A)^{-1}B\begin{bmatrix} 1 \\ 0 \end{bmatrix} \tag{5}$$

$$\frac{\hat{i}_o(s)}{\hat{v}_s(s)} = \begin{bmatrix} 0 & 0 & 0 & 0 & 0 & 0 & 2 \end{bmatrix}(sI-A)^{-1}B\begin{bmatrix} 0 \\ 1 \end{bmatrix} \tag{6}$$

B. Current and Voltage Feedback Signals

For cascade control, load voltage and current sensing is required; however, placing sensors on the secondary side at the electrochemical cell and feeding that information back to the control loop presents a challenge for two reasons. First, a high current sensor with good dynamics is required, which would be costly and take up a significant amount of space on the board. Second, the high current output requires a large surface area of copper on the PCB around which it would be difficult to route signal traces. It is preferable to sense these quantities on the primary side. The current is sensed using a small ac current sense transformer on the primary and the voltage is sensed from an auxiliary winding built into the transformer. Rectifying and filtering both signals then produces scaled estimates of the actual dc quantities. Figure 3 shows the method of extracting the current feedback signal i_{est} and the voltage signal v_{est}. The feedback signals i_{est} and v_{est} are estimates of the dc load current and load voltage.
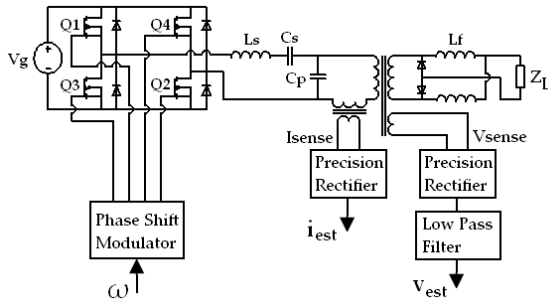

Fig. 3 SPRC with high side voltage and current sensing

The resulting i_{est} is related to the actual current output current i_{out} as follows:

$$\hat{i}_{est} = H_i \hat{i}_o \qquad (7)$$

where H_i is a scaling factor which includes the turns ratio of the main step down transformer and the current sense transformer, and a factor of 2 due to the current doubler at the output. This signal will also be amplified by a factor of 5 in the operational amplifier circuit to increase the signal-to-noise ratio. Additional filtering is not required since noise rejection is supplied by the current compensator in the control loop by design.

In the case of the voltage estimate, low pass filtering of the rectified signal is required because the voltage compensator (a PI compensator) does not provide high frequency noise rejection. Moreover, the voltage sensed on the transformer is not a scaled version of the output voltage due to the dynamics of the current doubler. The Thèvenin equivalent circuit for the output is shown in figure 4. From this circuit, the output voltage-to-secondary voltage transfer function, *OF*, can be derived as:

$$OF = \frac{\hat{v}_{sec}}{\hat{v}_o} = 2\left(1 + s\frac{L_f}{2Z_L}\right) \qquad (8)$$
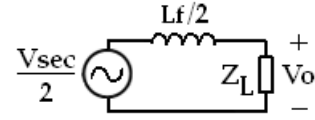

Fig. 4 Thevenin equivalent circuit of the output dc filter

H_v is a scaling factor including the number of turns of the secondary transformer winding N_s and auxiliary transformer winding N_{aux} and the gain of a resistor divider (1/2), which is required at the input to the precision rectifier to prevent saturation of the operational amplifiers.

$$H_v = \frac{1}{2}\frac{N_{aux}}{N_s} \qquad (9)$$

Then the estimated voltage is related to the output voltage by the following transfer function, which includes the low pass filter (LPF).

$$\frac{\hat{v}_{est}}{\hat{v}_o} = LPF \cdot \frac{1}{2}\frac{N_{aux}}{N_s} \cdot 2\left(1 + s\frac{L_f}{2Z_L}\right) \qquad (10)$$

III. CONTROL MODEL

Figure 5 shows the cascade control implementation that is used to control the voltage pulse applied to the electrochemical cell. The inner current loop limits the current through the electrochemical cell and facilitates the paralleling of power modules. The compensator for the inner current loop (G_{ci}) is a low pass filter. The compensator for the outer voltage loop (G_{fc}) is a proportional integral controller. The low pass filter (LPF) is a second order Butterworth filter. Z_L represents the impedance of the load.
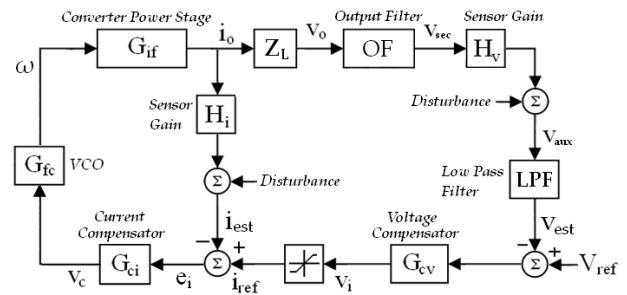

Fig. 5 Cascade control system with inner current control and outer voltage control loop

The control strategy uses frequency to control the output voltage. The frequency control signal v_c is converted to a clock signal using a voltage controlled oscillator (VCO). The VCO is implemented using the CD4046 chip. For a frequency range f_{max} = 145kHz and f_{min} = 100kHz and for V_{DD} = 15V, the small signal gain of the VCO is as follows:

$$G_{fc} = \frac{2\pi(f_{max} - f_{min})}{V_{DD}} = 6000\pi \qquad (11)$$

A. Current Compensator

From Bode plots of the frequency-to-output current transfer function G_{if} at full and half load it is found that the -3dB frequency (with respect to the dc gain) for each curve is greater than the switching frequency of the converter. Therefore, a pole is required in the current loop to bring the crossover frequency to a value less than $1/10^{th}$ the Nyquist frequency (50 kHz) of the converter. The current compensator transfer function will have the following form:

$$G_{ci} = K_{ci}\left(\frac{1}{s\tau_{ci}+1}\right) \tag{12}$$

From the Bode plots, the dc gain of G_{if} is -85.3dB. Multiplying this by G_{fc} and H_i gives a loop gain of 0.05. To minimize the error between the output current and reference current, K_{ci} should be designed for a gain greater than unity. Then, τ_{ci} can be designed to obtain the desired crossover frequency less than 5 kHz.

B. Voltage Compensator

With the above inner current loop compensation, the voltage controller can be designed around a new plant with transfer function given by:

$$\frac{\hat{v}_{out}(t)}{\hat{i}_{ref}(t)} = \frac{R_{eq}G_{if}G_{fc}G_{ci}}{1+G_{if}G_{fc}G_{ci}H_i} \tag{13}$$

The voltage compensator will be designed as a PI compensator with the following transfer function:

$$G_{cv} = K_{cv}\left(\frac{1+s\tau_{cv}}{s}\right) \tag{14}$$

This compensator produces infinite gain at dc so the output voltage will track the reference voltage. The output of this compensator is then the reference current signal. The zero of the compensator should be placed at a frequency less than $1/10^{th}$ of the crossover frequency so as not to introduce phase margin at the crossover frequency.

IV. SIMULATION & EXPERIMENTAL RESULTS

The specifications and ratings for the components for the power supply are shown in Table 1. The transformer has a rating of 500 W, operating frequency 100-145 kHz. It also has one turn auxiliary winding and one turn secondary winding.

TABLE I
Component values in SPRC

L_s (μH)	C_s (nF)	C_p (nF)	L_f (μH)	Transformer	V_g (V)
250	10	10	10	N= 48:1	350

Simulations and experiments have been performed on a resistive load and a simplified representation of the electrochemical load. This simplified representation is shown in the circuit diagram in figure 1. The electrolyte is represented by a resistor R_{elec} while each interface is represented by a capacitor C_{dl} in parallel with an interfacial resistance R_{int} that models the current flow due to the chemical reactions occurring at the interface between the electrode and the electrolyte. The simulated waveforms obtained using the resistive load differ only slightly compared to the ones obtained using the simple electrochemical cell equivalent circuit.

Fig. 6 shows the simulation results for the current loop for rated load and half rated load. For rated load, the crossover frequency is designed to be approximately 220Hz with a phase margin of 93°. For half rated load, the crossover frequency is 50Hz with a phase margin of 90°. Since the crossover frequency is low for each case, it can be seen that the current compensator provides sufficient noise rejection so that additional low pass filtering of the rectified current signal is not required. Fast rise time is accomplished with no overshoot in the full load case (100A) and very little overshoot at half rated load (50A).
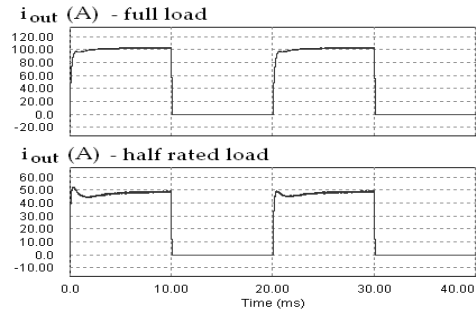

Fig. 6 Simulated output current for current loop control at rated load (top) and half rated load (bottom)

Figures 7 and 8 show the closed loop voltage control simulation results for full load and half rated load respectively. For the nominal load case in Fig. 7, the output current reaches 100A quickly while the output voltage ramps up slowly due to the charging of the double layer capacitors. For the half rated case, in Fig. 8, the current ramps up to 100A to charge the capacitors and then decays to 50A. As a result, the output voltage reaches rated voltage relatively quickly.
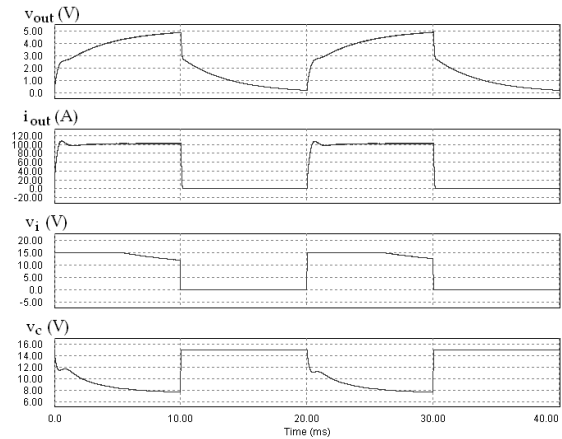

Fig. 7 Closed loop simulation results at nominal load

At the beginning of each pulse, the controller operation is nonlinear as the current command is clamped at an upper limit until the output voltage reaches a threshold (3 to 4V, depending on the loading) to move the controller into the linear regime. The current compensator is initialized to +15V at the beginning of each pulse to guarantee that the converter begins gating at the maximum rated switching frequency of 145 kHz. While the voltage compensator demands maximum rated current to bring the voltage up as quickly as possible, the response is limited by the dynamics of the current compensator, which is designed in such a way to prevent an overshoot as the switching frequency decreases toward the resonant frequency.
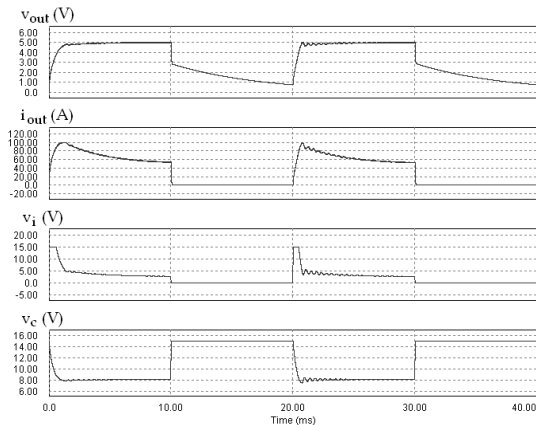

Fig. 8 Closed loop simulation results at half rated load

Figure 9 shows the salient waveforms of the voltage sensing circuit during steady state. The sensed voltage waveform (middle trace in figure 9) is the voltage across the auxiliary winding of the transformer which is proportional to the voltage across the primary winding and the parallel capacitor. An advantage of the series-parallel resonant converter is that the transformer voltage is sinusoidal which simplifies the construction of such a transformer. This voltage gets rectified (bottom trace in figure 9) using a high speed precision rectifier designed as in [9] and then filtered using a second order Butterworth filter to give the amplified estimated output voltage (top trace in figure 9).
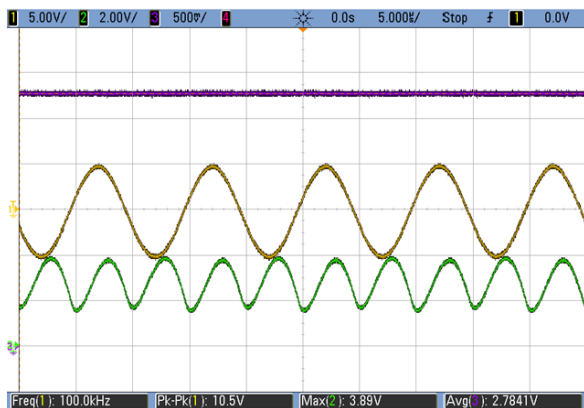

Fig. 9 Experimental results for the amplified estimated (top), sensed (middle) and rectified (bottom) voltages

Figure 10 shows a comparison of the measured experimental output dc voltage and the estimated output dc voltage under pulsed operation. The estimated voltage, obtained from rectifying, filtering and amplifying the auxiliary transformer voltage, has a steady state amplitude of 2.5V. The voltage is amplified by a factor of 2 in the logic circuit to improve the signal-to-noise ratio, so the actual estimated voltage is 1.25V. The steady state value of the estimated waveform is in good agreement with the actual output voltage, which was measured to be 1.27V. The main difference between these waveforms is that on turn on, there is a spike in the estimated voltage, which can be seen in figure 11. This spike corresponds to the dynamics of the output filter inductors which are accounted for in the controller design through the *OF* transfer function.
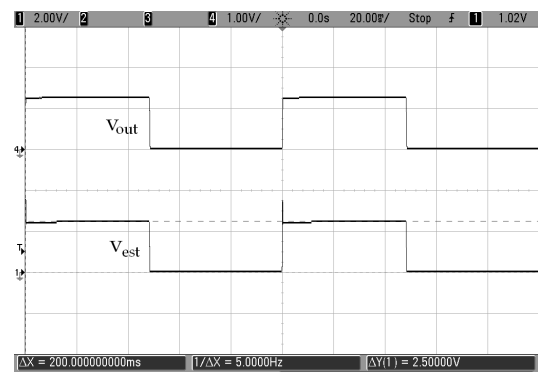

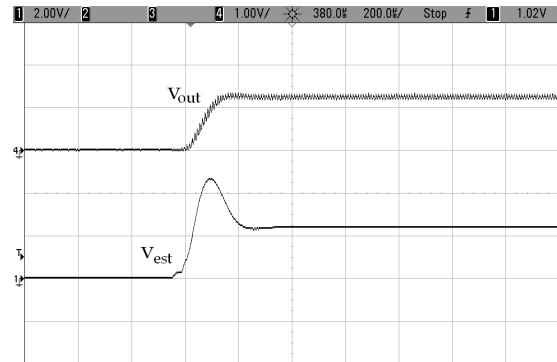Fig. 10 Actual and estimated experimental output voltage

Fig. 11 Magnification of actual and estimated experimental output voltage

Figure 12 shows the salient waveforms of the current sensing circuit during steady state. The sensed waveform (middle trace in figure 12) is the voltage across a sense resistor on the secondary of the current transformer. This voltage is proportional to the main transformer primary current (bottom trace in figure 12). The sensed signal is rectified (top trace in figure 12) using another high speed precision rectifier to give an estimation for the output current.

Fig. 13 shows the evolution of the parallel capacitor voltage and the output dc voltage at the beginning of a pulse. It can be seen that a continuous voltage transient (absence of discontinuous mode of operation) is

accomplished as expected due to the choice of Q for this converter [7].
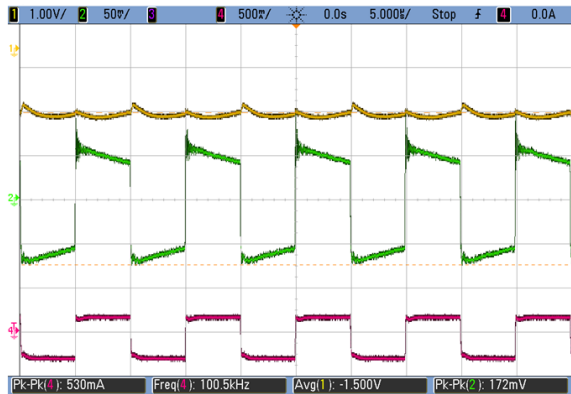

Fig. 12 Experimental results for the estimated (top), sensed (middle) and CT primary (bottom) currents
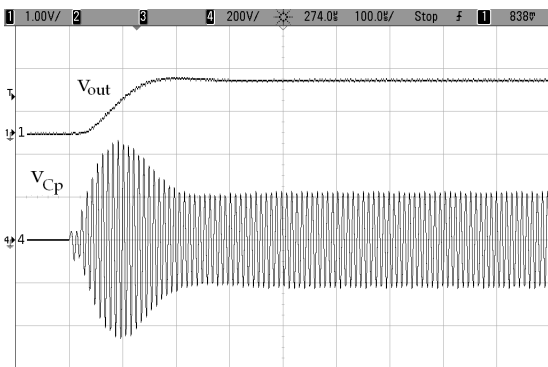

Fig. 13 Evolution of v_{out} and v_{Cp} at the beginning of a pulse

V. CONCLUSIONS

This paper has shown the feasibility of designing a cascade control loop structure for a pulsed series parallel resonant converter with a current doubler. The power supply consists of an inner current loop and an outer voltage loop. An inner current loop allows multiple converters to be placed in parallel in order to increase the output current and to prevent overcurrent protection. The outer voltage loop is used to control the electrochemical cell voltage. Estimates of the output dc voltage and dc current are obtained using information extracted from a current sensor connected in series with the primary of the output transformer and the voltage extracted from an auxiliary winding located on the output transformer. The switching frequency is used to control the output voltage.

ACKNOWLEDGMENT

REFERENCES

[1] M.S. Chandrasekar and M. Pushpavanam, "Pulse and pulse reverse plating—Conceptual advantages and applications," *Electrochim. Acta*, vol. 53, no. 8, pp. 3312-3322, March 2008.

[2] N. Ibl, "Some theoretical aspects of pulse electrolysis," *Surf. Technol.*, vol. 10, no. 2, pp. 81-104, Feb. 1980.

[3] J.C. Puippe and N. Ibl, "Influence of charge and discharge of electric double layer in pulse plating," *J. Appl. Electrochem.*, vol. 10, no. 5, pp. 775-784, Nov. 1980.

[4] K. Viswanathan et al, "The application of pulsed current electrolysis to a rotating-disk electrode system - 1. Mass Transfer," *J. Electrochem. Soc.*, vol. 125, no. 11, pp. 1772-1776, 1978.

[5] K. Viswanathan and H.Y. Cheh, "The application of pulsed current electrolysis to a rotating-disk electrode system - 2. Electrode Kinetics," *J. Electrochem. Soc.*, vol. 125, no. 10, pp. 1616-1618, 1978.

[6] K. Viswanathan and H.Y. Cheh, "Mass transfer aspects of electrolysis by periodic currents," *J. Electrochem. Soc.*, vol. 126, no. 3, pp. 398-401, 1979.

[7] K. Klement, F. P. Dawson, S. Thorpe, "Resonant converters for Pulsed Electrochemical Applications," 13th European Conference on Power Electronics and Applications, Sept 08-10, 2009, Barcelona, Spain.

[8] S.R. Sanders et al, "Generalized Averaging Method for Power Conversion Circuits," IEEE Trans. Power Electron., vol. 6, no. 2, April 1991.

[9] C.D. Ferris, *Elements of Electronic Design*, West Publishing Co.: Minnesota, 1995